photonics

MDPI

Article

Design and Simulation of Optical Waveguide Digital Adjustable Delay Lines Based on Optical Switches and Archimedean Spiral Structures

Ting An, Limin Liu *, Guizhou Lv, Chunhui Han, Yafeng Meng, Sai Zhu, Yuandong Niu and Yunfeng Jiang

Shijiazhuang Campus, Army Engineering University, Shijiazhuang 050003, China; anting@aeu.edu.cn (T.A.); lvgz@aeu.edu.cn (G.L.); hanch@aeu.edu.cn (C.H.); mengyf@aeu.edu.cn (Y.M.); zhus@aeu.edu.cn (S.Z.); niuyuandong@aeu.edu.cn (Y.N.); jyfoptics@aeu.edu.cn (Y.J.)

* Correspondence: liulimin0807@aeu.edu.cn

Abstract

In the field of modern optical communication, radar signal processing and optical sensors, true time delay technology, as a key means of signal processing, can achieve the accurate control of the time delay of optical signals. This study presents a novel design that integrates a 2 × 2 Multi-Mode Interference (MMI) structure with a Mach–Zehnder modulator on a silicon nitride–lithium niobate (SiN-$LiNbO_3$) heterogeneous integrated optical platform. This configuration enables the selective interruption of optical wave paths. The upper path passes through an ultralow-loss Archimedes' spiral waveguide delay line made of silicon nitride, where the five spiral structures provide delays of 10 ps, 20 ps, 40 ps, 80 ps, and 160 ps, respectively. In contrast, the lower path is straight through, without introducing an additional delay. By applying an electrical voltage, the state of the SiN-$LiNbO_3$ switch can be altered, facilitating the switching and reconfiguration of optical paths and ultimately enabling the combination of various delay values. Simulation results demonstrate that the proposed optical true delay line achieves a discrete, adjustable delay ranging from 10 ps to 310 ps with a step size of 10 ps. The delay loss is less than 0.013 dB/ps, the response speed reaches the order of ns, and the 3 dB-EO bandwidth is broader than 67 GHz. In comparison to other optical switches optical true delay lines in terms of the parameters of delay range, minimum adjustable delay, and delay loss, the proposed optical waveguide digital adjustable true delay line, which is based on an optical switch and an Archimedes' spiral structure, has outstanding advantages in response speed and delay loss.

Keywords: optical true delay line (OTDL); optical waveguide; Archimedes' spiral waveguide; optical path switching; thin-film lithium niobate (TFLN)

Received: 3 June 2025
Revised: 21 June 2025
Accepted: 27 June 2025
Published: 5 July 2025

Citation: An, T.; Liu, L.; Lv, G.; Han, C.; Meng, Y.; Zhu, S.; Niu, Y.; Jiang, Y. Design and Simulation of Optical Waveguide Digital Adjustable Delay Lines Based on Optical Switches and Archimedean Spiral Structures. *Photonics* **2025**, *12*, 679. https://doi.org/10.3390/photonics12070679

1. Introduction

In the domain of modern optical communication, radar signal processing and optical sensors, true time delay (TTD) technology, as a key means of signal processing, can achieve accurate control of the time delay of optical signals [1–3]. Consequently, it plays a crucial role in frontier fields such as phased-array radar [4–7], optical signal processing [8–10], optical communication systems [11–13], and quantum computing [14,15]. Nevertheless, traditional time delay technologies are typically constrained by the physical size, tuning range, and response speed of the device, rendering it challenging to satisfy the escalating demand for high-performance applications. Therefore, the development of a high-performance, digitally tunable true time delay line has emerged as one of the focal points of current

research. In recent years, research on optical true delay lines has mainly focused on four aspects: microring resonators [16–19], grating delay lines [20–22], multi-path switchable optical switches [23,24], and wavelength selective optical delay line [25–27].

Over the past few decades, multi-path switchable optical switches have been widely used in various photon integration platforms such as SOI [28–34], Si_3N_4 [35,36], PLC based on doped SiO_2 [37,38], polymer [39–41], and TFLN [42]. In the early stages, polymers were favored for optical switch delay line (OSDL) chips due to their distinctive advantages, such as straightforward fabrication processes, low optical loss, and cost-effectiveness [43]. However, this material exhibits notable drawbacks, including an excessively long switching time (on the order of milliseconds). Due to their low thermal conductivity, polymer-based switches consume high power consumption (up to hundreds of milliwatts per switch). Moreover, their inherently large heat capacity and low refractive index contrast result in bulky device sizes. Although the use of a specialized ethylene oxide polymer can facilitate rapid switching, it concomitantly introduces higher optical losses. Additionally, concerns regarding their long-term stability have been raised.

In recent years, the rapid development of optical waveguide technology have offered novel perspectives for realizing high-performance true time delay lines. Optical waveguide structure possess the merits of miniaturization, high integration, and low loss, effectively surmounting the limitations of traditional time delay devices [44,45]. Against this backdrop, Archimedes' spiral structure has attracted much attention due to its unique geometric characteristics. Archimedes' spiral, an equidistant spiral configuration, can significantly extend the optical path when applied in optical waveguides. This enables the achievement of a broader time delay range while maintaining a compact device footprint [46]. Furthermore, by incorporating a digital tuning mechanism, an Archimedes' spiral optical waveguide true time delay line can provide precise time delay control, thereby fulfilling the requirements of dynamic signal processing.

2. Theoretical Analysis

2.1. Optical True Time Delay

The core idea of optical true delay is to utilize the time difference in light propagation through paths of varying lengths to achieve a delay. Specifically, the propagation velocity of light in the waveguide can be expressed as follows:

$$v = \frac{c}{n} \tag{1}$$

In Equation (1), c represents the speed of light in a vacuum ($c \approx 3 \times 10^8$ m/s) and n is the refractive index of the waveguide material. Therefore, the time delay τ of the optical signal propagating in the waveguide can be calculated using the following formula:

$$\tau = \frac{L}{v} = \frac{L \cdot n}{c} \tag{2}$$

In Equation (2), L is the propagation path length of the optical signal in the waveguide.

The time delay in optical waveguides can be realized through the following approaches: (1) Altering the physical length of the waveguide: By designing waveguide paths with diverse lengths, different time delays can be achieved. For example, the spiral waveguide can introduce substantial time delays by extending the propagation path of the optical signal. In addition, the multilayer superposition structure can also prolong the propagation path by increasing the number of reflections of the optical signal [47]. (2) Employing microring resonator: Microring resonator, a specialized waveguide structure, enable optical signals to propagate back and forth within the ring cavity many times, thereby generating

significant time delays. Through rational design of the microring size and coupling coefficient, precise control over the optical signal time delay can be achieved [17,18]. For example, when the microring resonator is an over-coupled state, a positive time delay is obtained. (3) Utilizing optical switch: In certain adjustable delay lines, variable delays are realized by selecting different waveguide paths via optical switches. For example, a silicon-based 7-bit tunable optical delay line can select waveguide paths of varying lengths through optical switches, thus achieving up to 128 distinct delay states. In this study, a digital tunable delay line was designed and simulated on the SiN-$LiNbO_3$ hetero-integrated optical platform, leveraging the structure of optical switch and an Archimedes' spiral.

2.2. Time Delay Principle in Optical Waveguides

An optical waveguide is a structure designed to confine and direct the propagation of optical signals. Typically, it consists of a high-refractive-index core layer surrounded by a low-refractive-index cladding [48]. Light propagates within the waveguide through total internal reflection, thereby enabling low-loss optical transmission. The group refractive index of light is defined as the ratio of the speed of a light pulse or light group to the speed of light when a light wave propagates in the medium. The formula of group refractive index is as follows [49]:

$$n_g = n_{eff} - \lambda \frac{dn_{eff}}{d\lambda} \tag{3}$$

where n_{eff} represents the effective refractive index, and λ is the wavelength of light. $dn_{eff}/d\lambda$ denotes the rate of change of the refractive index with respect to the wavelength. This parameter is crucial in optical waveguide systems, as it directly influences the time delay and dispersion characteristics of optical signals. Understanding and accurately calculating the group refractive index is essential for optimizing the performance of optical delay lines and ensuring reliable data transmission in optical communication systems.

There is a close physical relationship between the group refractive index and group delay. Group delay refers to the time delay caused by the change in group velocity when a light pulse propagates through a medium. It can be expressed using the following formula:

$$\Delta t = \frac{L}{v_g} = \frac{n_g L}{c} \tag{4}$$

where L is the distance of light propagation in the medium.

2.3. Basic Principle of Archimedes' Spiral Optical Waveguide

The geometric expression of Archimedes' spiral is as follows:

$$r(\theta) = r_0 + \frac{\Lambda}{2\pi}\theta \tag{5}$$

where r_0 represents initial radius of the spiral, Λ is the pitch, and θ is the azimuth. Figure 1 shows five turns of Archimedes' spiral.

The Archimedes' spiral structure can extend the optical path in a confined space, effectively reducing the size of optical waveguide devices. By adjusting the parameters of the spiral (such as radius, number of turns, etc.), precise control over the optical path length can be achieved, enabling tunable time delays.

The field distribution of an Archimedes' spiral optical waveguide can be derived from its geometric characteristics and electromagnetic field theory. In optical waveguide, the light field distribution.is typically obtained by solving Maxwell's equations. For an Archimedes' spiral optical waveguide, the field distribution can be expressed as the superposition along

the spiral path. Assuming that the electric field distribution in the optical waveguide is $E(\tau, \theta, z)$, its general form can be expressed as follows:

$$E(\tau, \theta, z) = E_0(r) \cdot e^{i(l\theta - kz)} \quad (6)$$

where l represents the length of Archimedes' spiral optical waveguide, $E_0(r)$ is related to the wavelength of light, while λ is the wavelength of light.

As depicted in Figure 2, the heat distribution in the spiral waveguide is characterized by distinct patterns in both the top and side views. The top view shows the transverse distribution of the thermal field along the spiral path of the waveguide, with high-temperature regions concentrated on the inner side of the curved segments. The side view reveals the vertical distribution of the thermal gradient in the waveguide cross-section, indicating that heat is primarily dissipated toward the cladding.

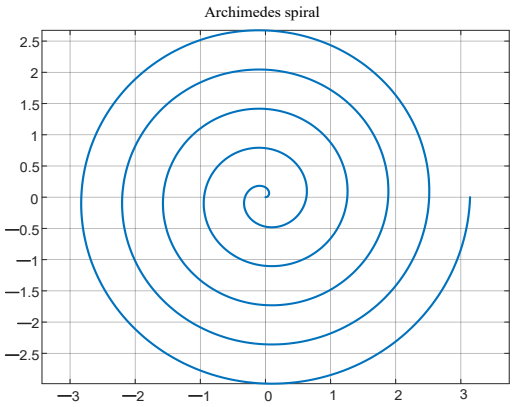

Figure 1. Archimedes' spiral structure (5 turns).

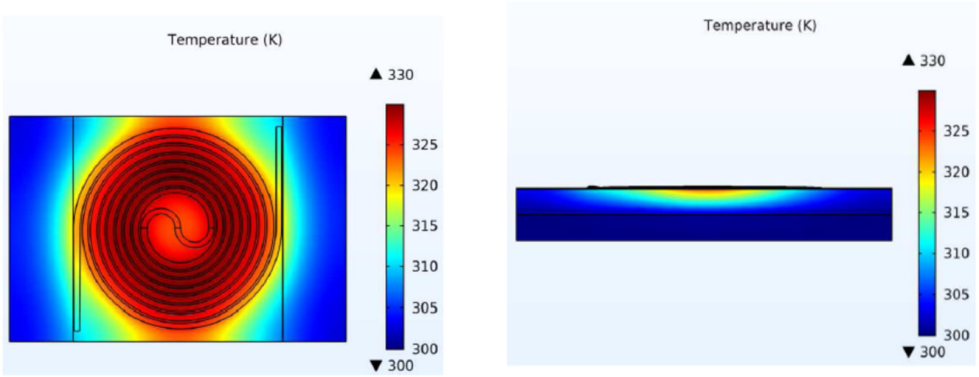

(**a**) (**b**)

Figure 2. The heat distribution in the spiral waveguide: (**a**) top view; (**b**) side view.

2.4. Digital Tunable Technology Based on Optical Switch

Digital tunable technology based on optical switch is a technology that manipulates the optical signal path through optical switch mechanisms to achieve the discrete adjustment of optical parameters, including time delay, dispersion, and filtering. Digital tuning of these parameters can be realized by designing selective switching of multiple paths or cascaded switches. This technology offers notable advantages such as discrete control, ease of integration, and straightforward programmability, thereby enabling rapid and accurate optical signal processing and regulation. In this study, a digital tunable true time delay line of optical waveguide based on an Archimedes' spiral structure is designed. The detailed design methodology and comprehensive simulation outcomes will be elaborated

in Section 3, providing in-depth insights into the technical feasibility and performance characteristics of the proposed design.

3. Design and Simulation of Optical Waveguide Digital Adjustable Delay Lines Based on Optical Switches and Archimedean Spiral Structures

3.1. Design Idea of Optical True Delay Line

In this study, a 2 × 2 Multi-Mode Interference (MMI) coupler, in conjunction with a Mach–Zehnder modulator, is employed to realize on-off selection of the optical path. The upper optical path traverses a silicon nitride waveguide spiral delay line with ultra-low loss characteristics. Specifically, five distinct spiral structures are designed to introduce delays of 10 ps, 20 ps, 40 ps, 80 ps, and 160 ps, respectively, thereby achieving a discrete adjustable delay ranging from 10 to 310 ps in 10 ps increments. Conversely, the lower path is a straight-through configuration, ensuring no additional delay is introduced. By applying voltage to alter the state of the lithium niobate switch, various combinations of these delay values can be realized, which constitutes the fundamental principle of the proposed digital adjustable delay line. Figure 3 illustrates the structural diagram of the digital tunable true delay line.

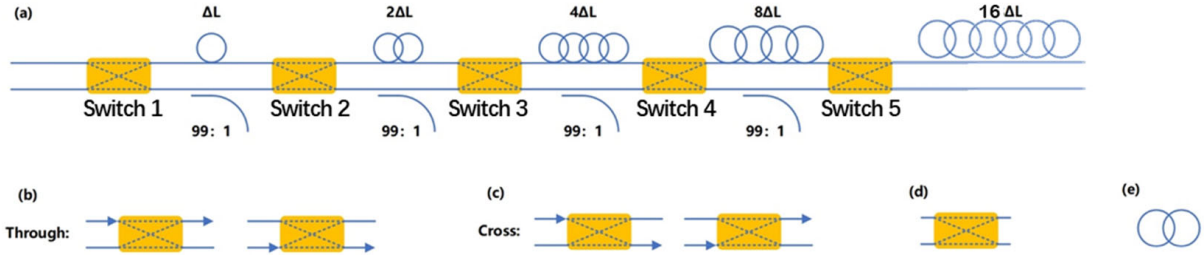

Figure 3. Digital adjustable true delay line. (**a**) Structure diagram. (**b**) "Through" switch state. (**c**) "Cross" switch state. (**d**) Switch unit. (**e**) Delay line unit.

As depicted in Figure 3, manipulating the switch state enables the combination of various delay values. By altering the state of the switch, it can realize the mutual combination of different delay amounts. Table 1 systematically presents the corresponding relationship between switch state and delay value.

The time delay of the Archimedes' waveguide spiral follows a pattern where it increases exponentially as the N power of 2. In this study, the designed delays are 10 ps, 20 ps, 40 ps, 80 ps, and 160 ps, respectively. By precisely controlling the through and cross states of the optical switch, this configuration can achieve optical true time delay with a minimum step of 10 ps, covering a range from 10 ps to 310 ps, as comprehensively summarized in Table 1.

Figure 4 shows the design layout of optical true delay lines. The layout features five optical switches integrated with five spiral waveguide delay structures, forming a compact and highly functional configuration. The chip size of the optical true delay line designed in this paper is less than 4 mm × 30 mm.

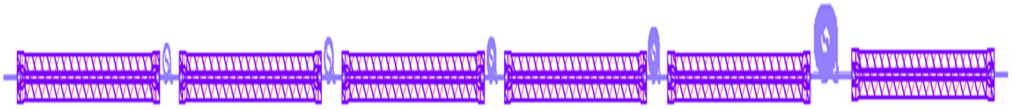

Figure 4. Design layout of optical true delay lines.

Table 1. Corresponding relationship between switch state and delay value.

Switch 1	Switch 2	Switch 3	Switch 4	Switch 5	Delay Value
through	cross	through	through	through	10 ps
cross	cross	cross	through	through	20 ps
through	through	cross	through	through	30 ps
cross	through	cross	cross	through	40 ps
through	cross	cross	cross	through	50 ps
cross	cross	through	cross	through	60 ps
through	through	through	cross	through	70 ps
cross	through	through	cross	cross	80 ps
through	cross	through	cross	cross	90 ps
cross	cross	cross	cross	cross	100 ps
through	through	cross	cross	cross	110 ps
cross	through	cross	through	cross	120 ps
through	cross	cross	through	cross	130 ps
cross	cross	through	through	cross	140 ps
through	through	through	through	cross	150 ps
cross	through	through	through	cross	160 ps
through	cross	through	through	cross	170 ps
cross	cross	cross	through	cross	180 ps
cross	through	cross	cross	cross	190 ps
cross	through	cross	cross	cross	200 ps
through	cross	cross	cross	cross	210 ps
cross	cross	through	cross	cross	220 ps
through	through	through	cross	cross	230 ps
cross	through	through	cross	through	240 ps
through	cross	through	cross	cross	250 ps
cross	cross	cross	cross	through	260 ps
through	through	cross	cross	through	270 ps
cross	through	cross	through	through	280 ps
through	cross	cross	through	through	290 ps
cross	cross	through	through	through	300 ps
through	through	through	through	through	310 ps

3.2. Specific Design

3.2.1. Design of SiN-$LiNbO_3$ Optical Switch

The Mach–Zehnder modulator, in conjunction with a 2 × 2 MMI structure, enables the realization of an optical transmission channel selection switch. An external voltage source applies a voltage to change the phase of the light wave to interfere with it and change the output port of the light wave, so as to realize the selection switch function on the optical transmission channel.

The losses associated with a 2 × 2 MMI typically include transmission losses, mode conversion losses, bending losses, coupling losses, and absorption losses inherent to the material. In this study, the Ansys Lumerical 2024 R1 software, employing the finite-difference time domain (FDTD) method, was utilized for comprehensive analysis. The MMI is equipped with a power monitor placed at the input and output end faces. By directly quantifying the power difference between the input and output, the total loss is directly obtained through $\alpha = 10\lg(P_{out}/P_{\text{in}})$. Simulation results indicated that the 2 × 2 MMI loss exhibits a total loss of less than 0.75 dB at a wavelength of 1550 nm.

Furthermore, by applying the following formula

$$PI = \frac{|P_{out1} - P_{out2}|}{P_{out1} + P_{out2}} \times 100\% \quad (7)$$

we obtained the power imbalance of a 2 × 2 MMI, and that is PI = 0.5 dB.

Regarding the optical switch integrated on TFLN material, the Pockels coefficient along its highest principal axis is significantly high. This coefficient is $r_{LiNbO_3} \approx 30 - 33\ pm/V$, over 300 times that of silicon ($r_{silicon} \approx 0.1\ pm/V$),endowing TFLN with unique electro-optic properties. When an electric field is applied, the refractive index of TFLN changes linearly with the electric field intensity. This linear electro-optic effect occurs without the need for carrier accumulation or nonlinear optical processes, enabling fast responses on the picosecond to nanosecond scale.

As reported in the study by Zhizhang Wang et al. from Nanjing University [50], the response speed of the optical switch can reach 14.4 ns, which is below 20 ns. Such a high-speed response significantly improves the fast-tuning ability of microwave beamforming.

Table 2 presents the structural parameters of the 2 × 2 MMI device. The main body size of MMI features dimensions of 76 μm × 10 μm × 0.5 μm, corresponding to its length, width and height (i.e., thickness), respectively. The width plays a crucial role in determining the number of modes within the multi-mode transmission region. For the silicon nitride waveguide employed in this study, a width of 10 μm enables the support of multiple transverse mode transmission. This characteristic facilitates the formation of a symmetrical output distribution following the interference process.

Table 2. Structural parameters of 2 × 2 MMI in this paper.

Component	Dimensions/Position	Thickness	Type
MMI	76 μm × 10 μm × 0.5 μm/(10 μm × 1 μm × 0.5 μm)	0.5 μm	Rectangle
Input waveguide_up	10 μm × 1 μm × 0.5 μm/(−15 μm, −1.75 μm, 0.15 μm)	0.5 μm	Rectangle
Input waveguide_down	10 μm × 1 μm × 0.5 μm/(−15 μm, −1.75 μm, 0.15 μm)	0.5 μm	Rectangle
Output waveguide_up	10 μm × 1 μm × 0.5 μm/(91 μm, 1.75 μm, 0.15 μm)	0.5 μm	Rectangle
Output waveguide_down	10 μm × 1 μm × 0.5 μm/(91 μm, −1.75 μm, 0.15 μm)	0.5 μm	Rectangle
Taper 1	(0 μm, 1.75 μm, 0.15 μm)	0.5 μm	Polygon
Taper 2	(0 μm, −1.75 μm, 0.15 μm)	0.5 μm	Polygon
Taper 3	(0 μm, 1.75 μm, 0.15 μm)	0.5 μm	Polygon
Taper 4	(0 μm, −1.75 μm, 0.15 μm)	0.5 μm	Polygon

The length of MMI is primarily governed by the interference effect and generally adheres to the following formula:

$$L = \frac{n_{eff} \cdot W^2}{4\lambda} \tag{8}$$

where n_{eff} is the effective refractive index, W is the waveguide width, and λ is the wavelength. The selected length of 76 μm satisfies the self-imaging condition at the wavelength of 1.55 μm, ensuring that the input light achieves power sharing or specific coupling at the output end. Meanwhile, the thickness of 0.5 μm aligns with the common thin-film silicon nitride processing standard. This parameter effectively balances the constraints of light field confinement and processing feasibility, while minimizing bending-induced optical loss.

A taper structure is employed to connect the standard waveguide and MMI body, minimizing mode mismatch loss through gradual adjustments in width and height. The four-dimensional symmetric design (comprising two pairs of positive/negative y-coordinates) ensures symmetry of input/output ports, thereby eliminating polarization-dependent loss.

The position of the light source is (−13 μm, 1.75 μm, 0 μm), with a size of 3 μm × 2 μm, and the wavelength of the light source is 1.5 μm–1.6 μm. The switch selection function is illustrated in Figure 5. An external voltage source applies an electrical signal to the Mach–Zehnder modulator, inducing a phase change in the light wave propagating through

its two arms. This phase alteration leads to interference between the two optical paths within the modulator, ultimately redirecting the light wave to a different output port. By precisely controlling the magnitude and polarity of the applied voltage, the optical signal can be selectively routed, thereby achieving the function of an optical switch that facilitates manipulation of light propagation paths in the designed delay line system. We also obtained the half-wave voltage of the switch, V_π, which is lower than 3 V.

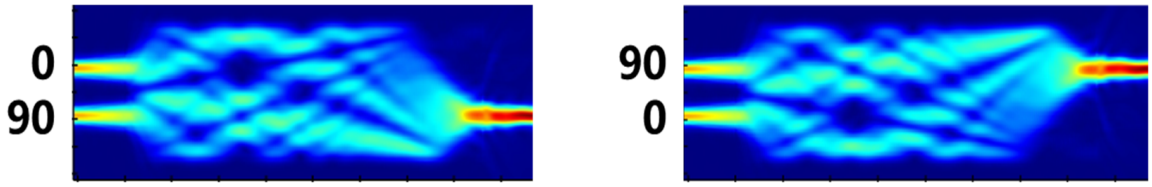

(**a**) (**b**)

Figure 5. Distribution of switch selection function field: (**a**) the phase of the lower arm is 90° (**b**) the phase of the upper arm is 90°.

3.2.2. Archimedes' Spiral Waveguide Delay Line

The phase change of optical waveguide is related to wavelength, group refractive index, and waveguide length, which satisfies the following formula:

$$\varphi(\omega) = -\frac{2\pi}{\lambda(\omega)} n_{eff}(\omega) L \tag{9}$$

The group delay is shown in Equation (8) below:

$$T_{group} = -\frac{\partial \varphi(\omega)}{\partial \omega} = \frac{L}{c}[n_{eff}(\omega) + \omega \frac{\partial n_{eff}(\omega)}{\partial \omega}] = \frac{L}{c} n_{group}(\omega) \tag{10}$$

According to simulation, the group refractive index of waveguide delay line is about 2.08. Archimedes' spiral optical waveguide lithography layout designed in this study is shown in Figure 6.

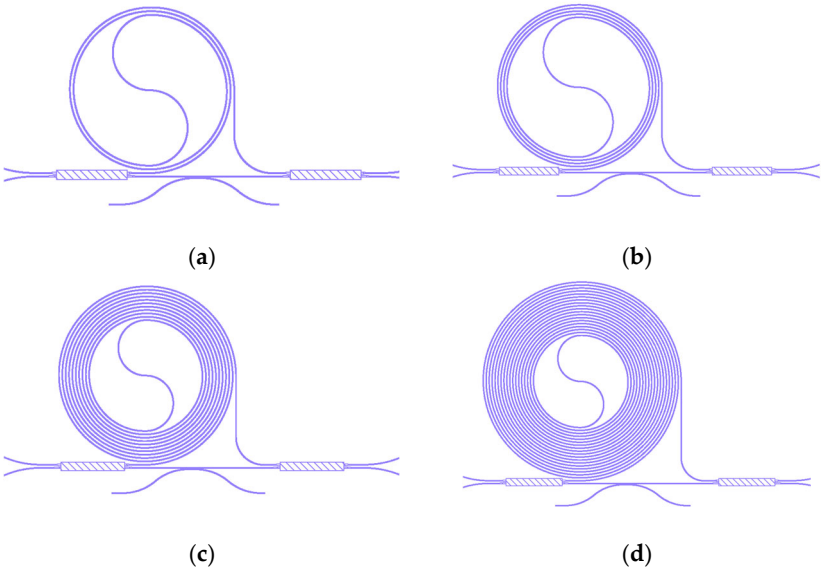

(**a**) (**b**)

(**c**) (**d**)

Figure 6. Archimedes' spiral waveguide delay line: (**a**) 10 ps delay, (**b**) 20 ps delay, (**c**) 40 ps delay, and (**d**) 80 ps delay.

The spiral waveguide delay line proposed in this study is designed for 1.5 μm–1.6 μm optically controlled beamforming networks, aiming to compensate for the aperture transition time required by each subarray. Constructed as a staggered Archimedes' spiral delay

line, the bending radius is constantly changing. Figure 6 depicts the chip design layout of the spiral waveguide at 1550 nm, taking an 80 ps delay structure as an example. Occupying an area of approximately 0.3 mm × 0.3 mm, the structure is composed of two groups of semicircles, one of which is used to lead the light into the center and the other is used to lead the light out for output. These inward and outward semicircles are connected by an S-shaped structure, and the radius of the structure remains large enough to achieve lossless transmission and mode position stability in the middle of the spiral waveguide. The time delay can be calculated according to the following formula:

$$t_d = \frac{n_g L}{c} \tag{11}$$

where t_d is the time delay of the spiral delay line, n_g is the effective index, and c is the speed of light. For the effective group index n_g of 1.62 (TE mode) and 1.51 (TM mode), the calculated delay time of the structure at 1550 nm precisely matches the designed value of 80 ps, validating the accuracy of the proposed design and theoretical model.

Table 3 list the structural parameters of spiral waveguide delay line designed in this study.

Table 3. Structural parameters of spiral waveguide delay line designed in this paper.

Material	Radius of Curvature	Waveguide Spacing
Silicon nitride	Spiral center: R_0 = 88.6 μm Outside the center: R(θ) = 88.6 + 0.637θ (μm)	Reverse waveguide spacing 4 μm Co-directional waveguide spacing 4 μm

3.2.3. Design and Simulation of Electrode

The electrode plays a key role in the performance, efficiency, stability and functionality of the device. The layout and material properties of the electrodes directly modulate the electric field distribution within the device. The strength and direction of the electric field can be optimized by reasonably designing the shape, size, and position of the electrode. The electrodes of the optical true delay line designed in this study are shown in Figure 7.

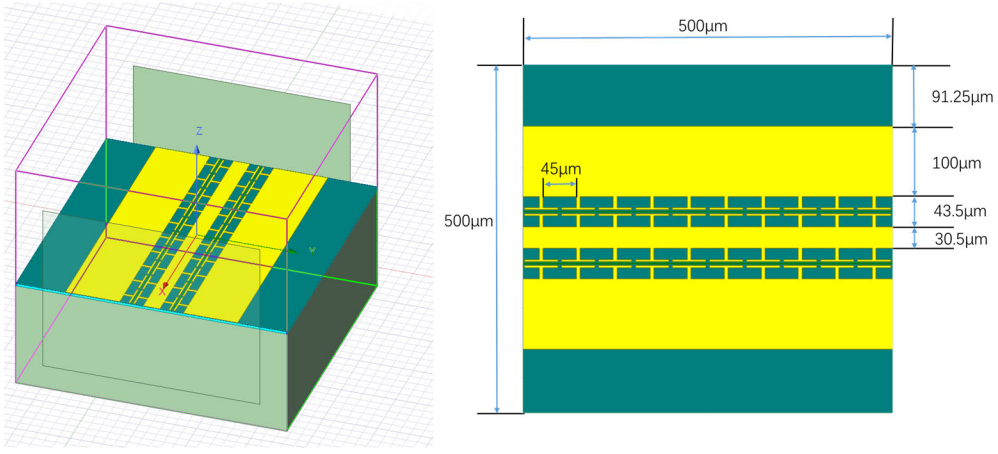

(**a**) (**b**)

Figure 7. Schematic diagram of electrode: (**a**) schematic diagram of the three-dimensional structure of the electrode; (**b**) schematic diagram of xoy cross-sectional structure.

Figure 7 provides a visual representation of their configuration and spatial arrangement. The overall size of the electrode is 500 μm × 500 μm. The purple line defines the spatial boundary, as shown in Figure 7a. The core structure is a two-dimensional

waveguide array extending along the X-axis, as shown in Figure 7b. The spacing between two adjacent units in the array is 45 µm.

As is shown in Figure 8, the materials from top to bottom are SiN, Gold, Lithium Niobate, and SOI. The base layer, constructed from Si material, has a thickness of 200 µm. The middle SOI layer, approximately 5 microns thick, serves as a crucial intermediate medium. Notably, the Lithium Niobate layer, with a thickness of 800 nm, plays a key role in the electro-optic modulation process due to its excellent electro-optic properties.

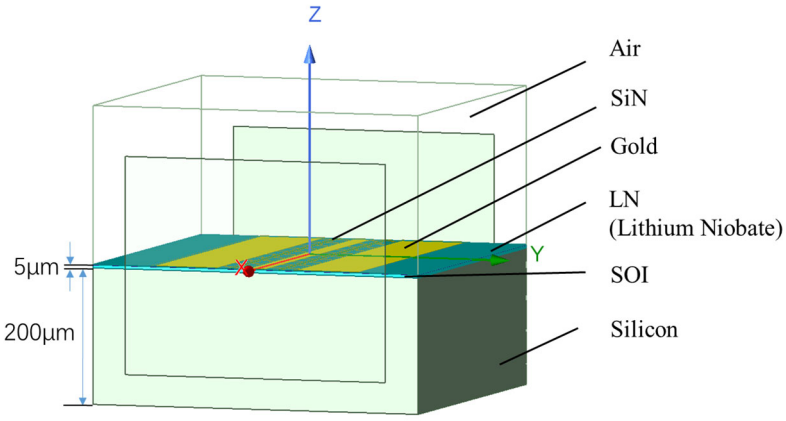

Figure 8. The material of the electrode and the thickness of various materials.

4. Result Analysis

4.1. Analysis of Delay Losses in Different Delay Times

An in-depth analysis of delay lines with varying delay times has been performed, as presented in Table 4. The total loss comprises transmission loss, bending loss, optical switch loss, and coupling loss. Its numerical change reflects the energy attenuation characteristics of the delay line under different delay requirements, and is the key index to evaluate the transmission efficiency of the system. Table 4 meticulously documents 31 sets of data, revealing that the total loss ranges from 2.1345 dB to 6.0398 dB. This range corresponds to the total losses of optical true time delay line systems with delay times ranging from 10 ps to 310 ps.

Table 4. The delay losses in different delay times.

Delay Time [ps]	Waveguide Length [cm]	Transmission Loss [dB]	Bending Times	Bending Loss [dB]	Optical Switch Loss [dB]	Coupling Loss [dB]	Total Loss [dB]
10	0.089	0.0445	9	0.09	1	1	2.1345
20	0.178	0.0890	17	0.17	1	1	2.2590
30	0.267	0.1335	26	0.26	1	1	2.3935
40	0.356	0.1780	34	0.34	1	1	2.5180
50	0.445	0.2225	43	0.43	1	1	2.6550
60	0.534	0.2670	51	0.51	1	1	2.7770
70	0.623	0.3115	60	0.60	1	1	2.9115
80	0.712	0.3560	69	0.69	1	1	3.0460
90	0.801	0.4005	78	0.78	1	1	3.1805
100	0.890	0.4450	86	0.86	1	1	3.3050
110	0.979	0.4895	95	0.95	1	1	3.4395
120	1.068	0.5340	103	1.03	1	1	3.5640
130	1.157	0.5785	112	1.12	1	1	3.6985
140	1.246	0.6230	120	1.20	1	1	3.8230
150	1.335	0.6675	129	1.29	1	1	3.9575
160	1.424	0.7120	137	1.37	1	1	4.0820
170	1.513	0.7565	146	1.46	1	1	4.2165
180	1.602	0.8010	154	1.54	1	1	4.3410
190	1.691	0.8455	163	1.63	1	1	4.4755
200	1.780	0.8900	171	1.71	1	1	4.6000

Table 4. *Cont.*

Delay Time [ps]	Waveguide Length [cm]	Transmission Loss [dB]	Bending Times	Bending Loss [dB]	Optical Switch Loss [dB]	Coupling Loss [dB]	Total Loss [dB]
210	1.869	0.9345	180	1.80	1	1	4.7345
220	1.958	0.9790	188	1.88	1	1	4.8590
230	2.047	1.0235	197	1.97	1	1	4.9935
240	2.136	1.0680	206	2.06	1	1	5.1280
250	2.225	1.1125	215	2.15	1	1	5.2625
260	2.314	1.1570	223	2.23	1	1	5.3870
270	2.403	1.2015	232	2.32	1	1	5.5215
280	2.492	1.2460	240	2.40	1	1	5.6460
290	2.581	1.2905	249	2.49	1	1	5.7805
300	2.670	1.3350	257	2.57	1	1	5.9050
310	2.759	1.3795	266	2.66	1	1	6.0398

Experimental observations indicate that total loss demonstrates a linear correlation with the increase in waveguide length and bending frequency. Notably, when the number of bends exceeds 200, the loss growth rate exhibits a marginal acceleration, potentially attributed to enhanced mode leakage caused by the reduction in waveguide bending radius. The loss variation fluctuates within the range of 0.1245 dB–0.1370 dB, with an average increment of about 0.13 dB per 10 ps delay. The incremental fluctuation is attributed to the coupling effect of nonlinearly increasing bending counts and transmission length. As the delay time increases from 10 ps to 310 ps, transmission loss increases from 0.0445 dB to 1.3795 dB, while the bending loss increases from 0.09 dB to 2.66 dB. Collectively, these two factors account for 76.5% of the total loss increment, establishing them as the primary contributors to loss degradation.

4.2. Analysis of the Overall Performance of Digital Dimmable True Delay Line

This study proposes a tunable optical true delay line based on the SiN-$LiNbO_3$ platform, featuring a maximum delay time of 310 ps and a resolution of 10 ps. In recent years, substantial theoretical investigations and experimental validations on multi-path switchable optical switches have been conducted by numerous scholars and research teams, yielding remarkable advancements in the field. A comparative analysis between the proposed work and related studies in the literature is presented in Table 5, highlighting the performance metrics and technical characteristics of different approaches.

Table 5. Performance comparison of tunable delay lines based on multi-path switchable optical switches.

Literature	Platform	Delay Tuning Step [ps]	Maximum Delay Tunable Range [ps]	Loss Delay Ratio [dB ns^{-1}]	Footprint [mm^2]
[29]	SOI	1.52	191.37	17.81	13.32
[36]	Si_3N_4	4.2	130	1.8	35
[37]	SiO_2	6	90.2	5.5	602
[38]	SiO_2	10,000	100,000	0.22	4166
[42]	TFLN	10	150	23	50
This work	SiN-$LiNbO_3$	10	310	13	120

The comparative analysis reveals that the delay range, maximum delay tunable range, and loss–delay ratio of optical true time delay lines are significantly influenced by their design structures and fabrication platforms. Notably, in terms of the maximum delay tunable range, the proposed design demonstrates an enhancement of over 60% compared to similar solutions (such as Literature [29]), effectively meeting a wider spectrum of delay adjustment requirements. Literature 38 focuses on long delay amounts; however, its tuning step size, as large as 10,000 ps, severely restricts the system's ability to perform fine-grained parameter adjustments. When compared with Literature [29] and Literature [42], the

proposed method not only outperforms in terms of the delay range but also exhibits a lower loss delay ratio, underscoring its superiority in achieving a better balance between delay performance and loss characteristics.

5. Conclusions

This study presents a tunable optical true delay line constructed on the SiN-$LiNbO_3$ platform, boasting a maximum delay time of 310 ps and a resolution of 10 ps. Benefiting from the linear electro-optic effect of TFLN, the response speed of the optical switch can be less than 20 ns. This remarkable performance significantly enhances the rapid tuning capabilities of microwave beamforming systems, enabling more agile and precise control over signal delays.

The proposed optical true delay line exhibits a distinct advantage in its low delay–loss ratio, a key performance metric indicating minimal signal attenuation per unit delay. This characteristic not only ensures efficient energy utilization within the device but also underscores its potential for high-fidelity signal transmission. As a core component in optoelectronics system, the low-loss and rapid-switching OTTD is expected to attract significant attention in strategic applications such as optical communications and microwave photonic radar systems. For future research directions, efforts will be concentrated on further reducing transmission losses by exploring advanced low-loss waveguide materials and optimizing waveguide bending structures.

Author Contributions: L.L. conceived the original idea and designed the research framework; T.A. and G.L. put forward the true time delay methodology; C.H. conducted simulations of spiral waveguides and verified the rationality of structures; Y.M. and Y.N. conducted formal analysis; S.Z. and Y.J. performed data curation; T.A. completed the initial draft writing; T.A. secured the research funding through Youth Independent Innovation Research Foundation. All authors have read and agreed to the published version of the manuscript.

Funding: This research was funded by Youth Independent Innovation Research Foundation, grant number KYSZJKQTZQ23013.

Institutional Review Board Statement: Not applicable.

Informed Consent Statement: Not applicable.

Data Availability Statement: The original contributions presented in this study are included in the article. Further inquiries can be directed to the corresponding author.

Acknowledgments: The authors have reviewed and edited the output and take full responsibility for the content of this publication.

Conflicts of Interest: The authors declare no conflicts of interest.

References

1. Wang, Y.; Dong, Z.; Ding, J.; Li, W.; Wang, M.; Zhao, F.; Yu, J. Photonics-assisted joint high-speed communication and high resolution radar detection system. *Opt. Lett.* **2021**, *46*, 6103–6106. [CrossRef] [PubMed]
2. Shi, S.; Niu, H.; Shi, W.; Lin, D.; Li, S.; Pan, S.; Yun, B. Integrated Optical Tunable Delay Line and Microwave Photonic Beamforming Chip: A Review. *Laser Photonics Rev.* **2024**, *19*, 202400663. [CrossRef]
3. Capmany, J.; Novak, D. Microwave photonics combines two worlds. *Nat. Photonics* **2007**, *1*, 319–330. [CrossRef]
4. Zhang, M.Y. *Optically Controlled Phased Array Radar*; National Defense Industry Press: Beijing, China, 2008; pp. 1–4.
5. Pan, S.L.; Zhang, Y.M. Microwave Photon radar and key technologies. *Sci. Technol. Rev.* **2017**, *35*, 36–52.
6. Pan, S.L.; Zhang, Y.M. Microwave Photonic Radar. *J. Light. Technol.* **2020**, *38*, 5450–5484. [CrossRef]
7. Sun, H.B.; Li, S.L.; Wang, Q.; Li, X.K. Development of phased array radar antenna delay technology. *J. Microw.* **2021**, *37*, 9–15.
8. Hu, C.; Luo, B.; Bai, W.L.; Pan, W.; Yan, L.; Zou, X. Stable radio frequency transmission of single optical source over fiber based on passive hase compensation. *IEEE Photonics J.* **2021**, *13*, 7200607. [CrossRef]

9. Lenz, G.; Eggleton, B.J.; Madsen, C.K.; Slusher, R.E. Optical delay lines based on optical filters. *IEEE J. Quantum Electron.* **2001**, *37*, 525–532. [CrossRef]
10. Liang, H.; Wang, K.; Han, S.; Mei, L.; Tian, Z.; Zhang, J.; Chong, M. Research on Delay and Bandwidth Expansion of Discrete Dispersive Fourier Transform in the Optical Domain. *Semicond. Optoelectron.* **2024**, *45*, 1–7.
11. Wang, H.; Chen, L.; Qi, Y.; Ba, D.; Dong, Y. Ultrafast microwave photonics frequency measurement technology. *Laser Optoelectron. Prog.* **2024**, *61*, 0112003.
12. Subha Priyadharshini, C.; Rajeswari, A. High-Capacity Optical Communication Systems using 4D Spatial-Wavelength-Zero Cross Correlation Encoding. *IETE J. Res.* **2025**, *1*, 1–13. [CrossRef]
13. Yessenov, M.; Bhaduri, B.; Delfyett, P.J.; Abouraddy, A.F. Free-space optical delay line using space-time wave packets. *Nat. Commun.* **2020**, *11*, 5782. [CrossRef]
14. Wu, Y.L.; Bao, W.S.; Cao, S.R.; Chen, F.; Chen, M.-C.; Chen, X.; Chung, T.-H.; Deng, H.; Du, Y. Strong quantum computational advantage using a superconducting quantum processor. *Phys. Rev. Lett.* **2021**, *127*, 180501. [CrossRef]
15. Jurcevic, P.; Jacadi-Abhari, A.; Bishop, L.S.; Lauer, I.; Bogorin, D.F.; Brink, M. Demonstration of quantum volume 64 on a superconducting quantum computing system. *Quantum Sci. Technol.* **2021**, *6*, 025020. [CrossRef]
16. Bliek, L.; Wahls, S.; Visscher, I.; Taddei, C.; Timens, R.B.; Oldenbeuving, R.M.; Roeloffzen, C.G.H.; Verhaegen, M. Automatic Delay Tuning of a Novel Ring Resonator-Based Photonic Beamformer for a Transmit Phased Array Antenna. *J. Light. Technol.* **2019**, *37*, 346–348. [CrossRef]
17. Xiang, C.; Davenport, M.L.; Khurgin, J.B.; Morton, P.A.; Bowers, J.E. Low-Loss continuously tunable optical true time delay based on Si3N4 ring resonators. *IEEE J. Sel. Top. Quantum Electron.* **2018**, *24*, 1–9. [CrossRef]
18. Shan, W.; Lu, L.; Wang, X.; Zhou, G.; Liu, Y.; Chen, J.; Zhou, L. Broadband continuously tunable microwave photonic delay line based on cascaded silicon microrings. *Opt. Express* **2021**, *29*, 3375. [CrossRef] [PubMed]
19. Xue, X.X.; Xuan, Y.; Bao, C.Y.; Li, S.; Zheng, X.; Zhou, B. Microcomb-based true-time delay network for microwave beamforming with arbitrary beam pattern control. *J. Light. Technol.* **2018**, *36*, 2312–2321. [CrossRef]
20. Sun, H.; Wang, Y.; Chen, L.R. Integrated discretely tunable optical delay line based on step-chirped subwavelength grating waveguide bragg gratings. *J. Light. Technol.* **2020**, *38*, 5551–5560. [CrossRef]
21. Srivastava, N.K.; Parihar, R.; Raghuwanshi, S.K. Efficient photonic beamforming system incorporating a unique featured tunable chirped fiber Bragg grating for application extended to the ku-band. *IEEE Trans. Microw. Theory Tech.* **2020**, *68*, 1851–1857. [CrossRef]
22. Perez-lopez, D.; Sanchez, E.; Capmany, J. Programmable true time delay lines using integrated waveguide meshes. *J. Light. Technol.* **2018**, *36*, 4591–4601. [CrossRef]
23. Zhu, C.; Lu, L.; Shan, W.; Xu, W.; Zhou, G.; Zhou, L.; Chen, J. Silicon integrated microwave photonic beamformer. *Optica* **2020**, *7*, 1162. [CrossRef]
24. Sun, X.H. True Time-Delay Optical Beamforming Technology with Optic Switched Differential Structure and its Application in Radar Target Direction Finding. Master's Thesis, Zhejiang University, Hangzhou, China, 2022; pp. 41–48.
25. Duan, X.; Zhang, S.T.; Jiang, Y.Y. Improvement and implementation of a multi-channel programmable optical controlled true time delay network. *Opt. Commun. Technol.* **2017**, *41*, 1–4.
26. Niu, X.Y.; Gu, Y.R.; Chu, X.; Yao, J.; Yao, J.; Yi, M.; Wang, L. Primary study on time control technology of active phasedarray based on photoconductive microwave source. *High Power Laser Partical Beams* **2023**, *36*, 1–6.
27. Tessema, N.M.; Cao, Z.; Zantvoort, J.H.C.V.; Mekonnen, K.A.; Trinidad, A.M.; Tangdiongga, E.; Smolders, A.B.; Koonen, A.M.J. Wavelength-dependent Continuous Delay Based on a Si_3N_4 Optical Ring Resonator for K-band Radio Beamformer. In Proceedings of the IEEE International Topical Meeting on Microwave Photonics, California, CA, USA, 31 October–3 November 2016; IEEE: Piscataway, NJ, USA, 2016; pp. 305–308.
28. Xie, J.; Zhou, L.; Li, Z.; Wang, J.; Chen, J. Seven-bit reconfigurable optical true time delay line based on silicon integration: Erratum. *Opt. Express* **2014**, *22*, 25516. [CrossRef]
29. Zheng, P.F.; Wang, C.Q.; Xu, X.M.; Li, J.; Lin, D.D.; Hu, G.H. A Seven Bit Silicon Optical True Time Delay Line for Ka-Band Phased Array Antenna. *IEEE Photonics J.* **2019**, *11*, 1–9. [CrossRef]
30. Zheng, P.F.; Xu, X.M.; Lin, D.D.; Liu, P.C.; Hu, G.H.; Yun, B.F. A wideband 1×4 optical beam-forming chip based on switchable optical delay lines for Ka-band phased array. *Opt. Commun.* **2021**, *488*, 126842. [CrossRef]
31. Zhang, L.; Hong, S.H.; Wang, Y.; Yan, H.; Xie, Y.; Chen, T.; Zhang, M.; Yu, Z.; Shi, Y.; Liu, L.; et al. Ultralow-Loss Silicon Photonics beyond the Singlemode Regime. *Laser Photonics Rev.* **2022**, *16*, 2100292. [CrossRef]
32. Shi, S.Q.; Hu, G.H.; Lin, D.D.; Zhang, J.Y.; Liu, P.C.; Lu, M.J.; Cheng, W.; Lin, T.; Yun, B.F.; Cui, Y.P. Performance comparison of integrated optical switching delay lines on three typical photonic integration pilot lines. *Opt. Laser Technol.* **2023**, *159*, 109016. [CrossRef]
33. Xie, Y.W.; Hong, S.H.; Yan, H.; Zhang, C.P.; Zhang, L.; Zhuang, L.M.; Dai, D.X. Low-loss chip-scale programmable silicon photonic processor. *Opto-Electron. Adv.* **2023**, *6*, 220030. [CrossRef]

34. Fathpour, S.; Riza, N. Silicon-photonics-based wideband radar beamforming: Basic design, Optical. *Engineering* **2010**, *49*, 018201. [CrossRef]
35. Moreira, R.L.; Garcia, J.; Li, W.; Bauters, J.; Barton, J.S.; Heck, M.J.R.; Bowers, J.E.; Blumenthal, D.J. Integrated Ultra-Low-Loss 4-Bit Tunable Delay for Broadband Phased Array Antenna Applications. *IEEE Photonics Technol. Lett.* **2013**, *25*, 1165–1168. [CrossRef]
36. Lin, D.; Shi, S.; Liu, P.; Cheng, W.; Lu, M.; Lin, T.; Hu, G.; Yun, B.; Cui, Y. Low loss silicon nitride 1 × 4 microwave photonic beamforming chip. *Opt. Express* **2022**, *30*, 30672–30683. [CrossRef]
37. Song, Q.Q.; Hu, Z.F.; Chen, K.X. Scalable and reconfigurable true time delay line based on an ultra-low-loss silica waveguide. *Appl. Opt.* **2018**, *57*, 4434–4439. [CrossRef] [PubMed]
38. Liu, D.P.; Sun, S.Q.; Yin, X.; Sun, B.; Sun, J.; Liu, Y.; Li, W.; Zhu, N.; Li, M. Large-capacity and low-loss integrated optical buffer. *Opt. Express* **2019**, *27*, 11585–11593. [CrossRef]
39. Howley, B.; Wang, X.; Chen, M.; Chen, R.T. Reconfigurable Delay Time Polymer Planar Lightwave Circuit for an X-band Phased-Array Antenna Demonstration. *J. Light. Technol.* **2007**, *25*, 883–890. [CrossRef]
40. Wang, X.L.; Howley, B.; Chen, M.Y.; Chen, R.T. Phase error corrected 4-bit true time delay module using a cascaded 2 × 2 polymer waveguide switch array. *Appl. Opt.* **2007**, *46*, 379–383. [CrossRef]
41. Pan, Z.; Subbaraman, H.; Lin, X.; Li, Q.; Zhang, C.; Ling, T.; Guo, L.J.; Chen, R.T. Laser Science to Photonic Applications. In Proceedings of the Conference on Lasers and Electro-Optics (CLEO), San Jose, CA, USA, 8–13 June 2014.
42. Ke, W.; Lin, Y.; He, M.; Xu, M.; Zhang, J.; Lin, Z.; Yu, S.; Cai, X. Digitally tunable optical delay line based on thin-film lithium niobate featuring high switching speed and low optical loss. *Photonics Res.* **2022**, *10*, 2575–2583. [CrossRef]
43. Chen, R.T. Polymer-based photonic integrated circuits. *Opt. Laser Technol.* **1993**, *25*, 347–365. [CrossRef]
44. Hong, S.; Zhang, L.; Wu, J.; Peng, Y.; Lyu, L.; Hu, Y.; Xie, Y.; Dai, D. Multimode-enabled silicon photonic delay lines: Break the delay-density limit. *Light Sci. Appl.* **2025**, *14*, 145. [CrossRef]
45. Wang, X.; Zhou, L.; Li, R.; Xie, J.; Lu, L.; Wu, K.; Chen, J. Continuously tunable ultra-thin silicon waveguide optical delay line. *Optica* **2017**, *4*, 507–515. [CrossRef]
46. Hong, S.H.; Zhang, L.; Wang, Y.; Zhang, M.; Xie, Y.; Dai, D. Ultralow-loss compact silicon photonic waveguide spirals and delay lines. *Photonics Res.* **2022**, *10*, 1–7. [CrossRef]
47. Ma, T.; Ma, M.; Guo, L.J. Optical multilayer thin film structure inverse design: From optimization to deep learning. *iScience* **2025**, *28*, 112222. [CrossRef]
48. Trager, F. *Modern Optics and Photonics Technology*; Springer: Berlin/Heidelberg, Germany, 2012.
49. Liu, S.; Li, C. *Photonics Technology and Application*; Guangdong Science and Technology Press: Guangzhou, China, 2006.
50. Wang, Z.Z.; Li, X.Y.; Ji, J.T.; Sun, Z.; Sun, J.; Fang, B.; Lu, J.; Li, S.; Ma, X.; Chen, X.; et al. Fast-speed and low-power-consumption optical phased array based on lithium niobate waveguides. *Nanophotonics* **2024**, *13*, 2429–2436. [CrossRef]